ACS Infectious Diseases

Article

pubs.acs.org/journal/aidcbc

Structural and Functional Survey of Environmental Aminoglycoside Acetyltransferases Reveals Functionality of Resistance Enzymes

Zhiyu Xu,[†] Peter J. Stogios,[†,‡] Andrew T. Quaile,[†] Kevin J. Forsberg,[§,◆] Sanket Patel,[§,⊥] Tatiana Skarina,[†,‡] Scott Houliston,[¶] Cheryl Arrowsmith,[¶] Gautam Dantas,[§,⊥,∥,▽] and Alexei Savchenko*[,†,‡,○]

[†]Department of Chemical Engineering and Applied Chemistry, University of Toronto, 200 College Street, Room 333, Toronto, Ontario M5S 3E5, Canada

[‡]Center for Structural Genomics of Infectious Diseases (CSGID), Health Research Innovation Center, 3280 Hospital Drive NW, Calgary, Alberta T2N 4N1, Canada

[§]Center for Genome Sciences & Systems Biology, Washington University School of Medicine, 4515 McKinley Avenue, Room 5314, St. Louis, Missouri 63110, United States

[⊥]Department of Pathology and Immunology, Washington University School of Medicine, 660 S. Euclid Avenue, St. Louis, Missouri 63110, United States

[¶]Department of Medical Biophysics, University of Toronto, 101 College Street, Room 4-601, Toronto, Ontario M5G 1L7, Canada

[∥]Department of Biomedical Engineering, Washington University in St. Louis, 1 Brookings Drive, St. Louis, Missouri 63130-6100, United States

[▽]Department of Molecular Microbiology, Washington University School of Medicine, 660 S. Euclid Avenue, St. Louis, Missouri 63110, United States

[○]Department of Microbiology, Immunology and Infectious Diseases, University of Calgary, 2C66 Health Research Innovation Center, 3280 Hospital Drive NW, Calgary, Alberta T2N 4N1, Canada

Supporting Information

ABSTRACT: Aminoglycoside *N*-acetyltransferases (AACs) confer resistance against the clinical use of aminoglycoside antibiotics. The origin of AACs can be traced to environmental microbial species representing a vast reservoir for new and emerging resistance enzymes, which are currently undercharacterized. Here, we performed detailed structural characterization and functional analyses of four metagenomic AAC (meta-AACs) enzymes recently identified in a survey of agricultural and grassland soil microbiomes (Forsberg et al. *Nature* 2014, *509*, 612). These enzymes are new members of the Gcn5-Related-*N*-Acetyltransferase superfamily and confer resistance to the aminoglycosides gentamicin C, sisomicin, and tobramycin. Moreover, the meta-AAC0020 enzyme demonstrated activity comparable with an AAC(3)-I enzyme that serves as a model AAC enzyme identified in a clinical bacterial isolate. The crystal structure of meta-AAC0020 in complex with sisomicin confirmed an unexpected AAC(6′) regiospecificity of this enzyme and revealed a drug binding mechanism distinct from previously characterized AAC(6′) enzymes. Together, our data highlights the presence of highly active antibiotic-modifying enzymes in the environmental microbiome and reveals unexpected diversity in substrate specificity. These observations of additional AAC enzymes must be considered in the search for novel aminoglycosides less prone to resistance.

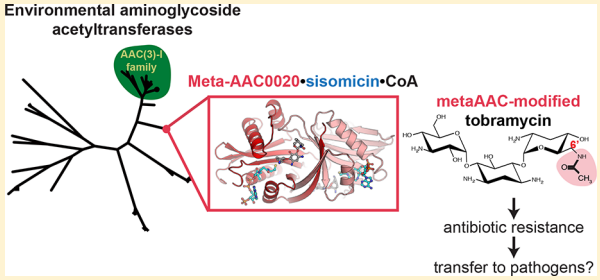

KEYWORDS: *antibiotic resistance, resistome, aminoglycosides, acetyltransferase, environmental, crystal structure*

Antibiotic resistance poses a long-term challenge to health, agriculture, and economic development, threating to become a global public health crisis overshadowing recent viral outbreaks.[2] In response to this threat, surveillance is one of the pillars of the strategy adopted by multiple countries, whereby antibiotic-resistant organisms and their resistance genes are to be rapidly detected and their presence communicated through the medical and scientific community.[2]

A basic research aspect of such surveillance efforts is to identify and understand the source of antibiotic resistance genes (ARGs). It is known that antibiotic resistance can arise through intrinsic resistance (i.e., genes or cellular structures such as the outer membrane that are native to bacteria and

Received: May 3, 2017
Published: July 30, 2017

DOI: 10.1021/acsinfecdis.7b00068
ACS Infect. Dis. 2017, 3, 653−665

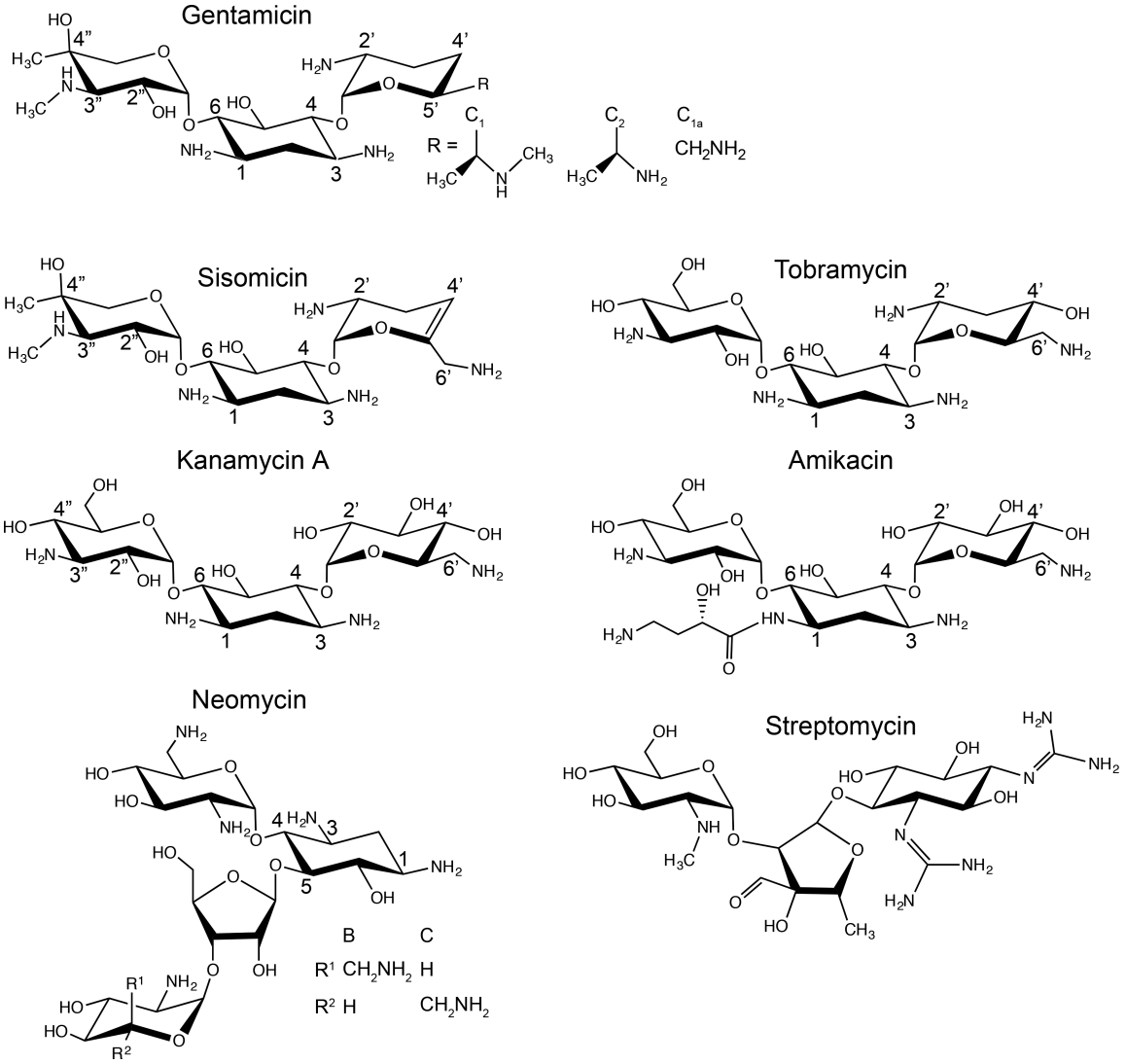

Figure 1. Chemical structures of aminoglycosides.

provide protection from antibiotics) or through the acquisition of foreign genes encoding the resistance functionality by horizontal gene transfer.[3] The evolutionary origin of ARGs has been traced to the environmental organisms producing these molecules as part of their interspecies survival strategy or to benign bacteria that occupy overlapping niches with the producers. Selection pressure by antibiotics encourages the mobilization and dissemination of ARGs between bacteria through horizontal gene transfer.[4] Ultimately, ARGs are discovered in human pathogens but too often this discovery is found in a multidrug resistant and difficult-to-treat infection. Thus, identification of ARGs in environmental microbial communities may allow for a more predictive and actionable understanding of clinical resistance. Characterization of environmental ARGs would allow for linking clinical resistance with the environmental resistome, allow evaluation of the potential of these environmental genes to evolve into clinically important ARGs, and provide targets for surveillance of potential new and emerging antibiotic resistance determinants.

Aminoglycosides are a major class of antibiotic introduced in 1944[5] and widely used in the treatment of serious diseases caused by Gram-negative bacteria.[6,7] However, the efficacy of aminoglycosides is often compromised by resistance. Inactivation by aminoglycoside-modifying enzymes is the most common mechanism of resistance.[8] Of such enzymes, aminoglycoside *N*-acetyltransferases (AACs), which modify the amino groups at four positions (AAC(1), (3), (2′), and (6′)) of the aminoglycoside scaffold, include the most number of catalogued variants.[8] Other classes of aminoglycoside-modifying enzymes include aminoglycoside *O*-phosphotransferases (APHs) and aminoglycoside *O*-nucleotidyltransferases (ANTs),[7] and these also contribute to clinical aminoglycoside resistance. However, AACs are the main source of clinical resistance of Gram-negative pathogenic bacteria to essentially all clinically relevant aminoglycosides.[7,8]

To date, there have been more than 70 AACs identified in pathogens, demonstrating the spread of this resistance mechanism.[8] Many *aac* genes are encoded in mobile genetic elements (i.e., plasmids, transposons, and integrons), which facilitate their dissemination, and are found colocalized with ARGs for other classes of antibiotics, such as β-lactamases.[8] In other instances, *aac* genes are chromosomal and thus provide intrinsic resistance and/or represent evolutionary antecedents to mobilized resistance genes.[9−11] While AACs have been widely detected in clinical isolates, their presence in environmental bacteria, which may represent the ultimate reservoir and

DOI: 10.1021/acsinfecdis.7b00068
ACS Infect. Dis. 2017, 3, 653−665

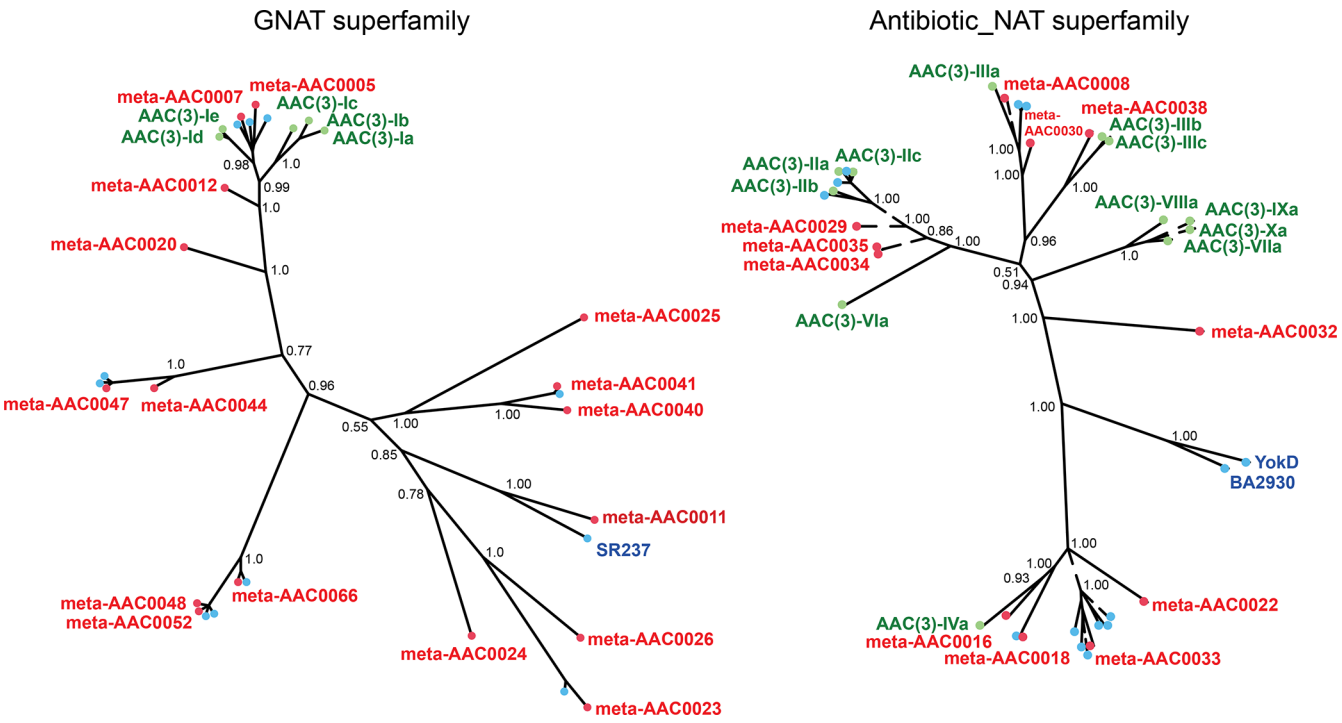

Figure 2. Phylogenetic reconstruction of meta-AAC sequences. meta-AAC sequences fall into the two families GNAT and Antibiotic_NAT. Sequences labeled with green, red, and blue correspond to clinical isolates of AAC(3) enzymes, meta-AAC proteins, and those that have been previously crystallized, respectively.

source of these enzymes, has remained relatively uncharacterized.

A functional metagenomic investigation by Forsberg et al. of environmental soil samples discovered diverse genes that confer resistance to many classes of antibiotics including aminoglycosides.[1] This study showed that metagenomic ARGs can be nearly identical in sequence with those of clinical ARGs, clearly linking these two classes of ARGs. However, this study also showed that the environment is a rich course of sequence-divergent ARGs, suggesting different or even novel molecular mechanisms of resistance. Twenty-seven genes that conferred resistance to the aminoglycoside gentamicin were predicted to encode AAC enzymes based on sequence similarity, representing a spectrum of the environmental resistome against aminoglycosides. However, these enzymes were not characterized for specificity or enzymatic efficiency, and therefore, their suitability to mediate clinically relevant levels of resistance and the functional relationship between clinically isolated and environmental AACs remains unclear.

In this study, we performed structural and functional characterization of environmental AAC enzymes (which we term meta-AACs) which were previously discovered via functional metagenomic selections.[1] Our results show that these enzymes possess efficiency that rivals AAC enzymes isolated from human pathogens and thus indeed represent a "primed" environmental reservoir of aminoglycoside resistance. We also show that one meta-AAC recognizes aminoglycosides in a manner distinct from characterized AACs, thus confirming that the environment provides a rich source of novel AACs.

RESULTS

Four meta-AAC Enzymes Share Sequence Similarity with Resistance Enzymes from Clinical Isolates. The functional metagenomics screening of soil microbial communities that identified over two dozen metagenomic AAC (meta-AACs) enzymes utilized a low (16 μg/mL) concentration of gentamicin to identify heterologous resistance in *E. coli*.[1] The potential of these enzymes to mediate clinical levels of resistance and molecular determinants of function was not further characterized.

According to the NCBI Conserved Domain Database, of these 27 meta-AACs, 16 belong to the Gcn5-related *N*-acetyltransferase (GNAT) protein superfamily while 11 are part of the Antibiotic *N*-acetyltransferase (Antibiotic_NAT) protein superfamily. Since involvement of representatives of the latter family in clinical resistance remains poorly charaterized, we focused on meta-AAC members of the GNAT superfamily. Many GNAT superfamily enzymes have been functionally and structurally characterized as *bona fide* AAC enzymes isolated from human pathogens (reviewed in refs 12 and 13); we therefore performed a comparative analysis between such clinical and meta-AACs. Phylogenetic reconstruction (Figure 2) revealed that the identified meta-AACs belong to diverse clades within the GNAT superfamily, reflecting their substantial primary sequence variation (e.g., the meta-AAC0005 and meta-AAC0011 enzymes share only 18% sequence identity). Nevertheless, the meta-AAC0005 and meta-AAC0007 enzymes and to a lesser extent the meta-AAC0012 and meta-AAC0020 sequences formed a nested clade with AAC(3)-Ia, -Ib, -Ic, -Id, and -Ie, five key AAC enzymes from pathogens,[8] prompting us to suggest that these four meta-AACs may share functional properties of AAC(3) enzymes. To compare the properties of clinical and meta-AACs, we proceeded with detailed functional and structural characterization of these four meta-AAC enzymes.

meta-AACs Confer High-Level Heterologous Resistance to Several Aminoglycosides. To test the ability of meta-AAC enzymes to confer resistance to aminoglycoside

DOI: 10.1021/acsinfecdis.7b00068
ACS Infect. Dis. 2017, 3, 653−665

antibiotics, we subjected an *E. coli* (Δ*bamB* Δ*tolC*) strain[14] expressing individual meta-AAC enzymes to the Kirby-Bauer antibiotic susceptibility test[15] against a panel of seven aminoglycoside antibiotics representing distinct chemical configurations within this general antibiotic class (Figures 1 and 3). The same *E. coli* strain expressing the AAC(3)-Ib enzyme was tested as a reference for an AAC derived from a pathogen. All four tested meta-AAC enzymes conferred resistance to gentamicin and sisomicin even at the highest tested concentration (135 μg/mL), except for meta-AAC0020, which conferred sisomicin resistance only up to 45 μg/mL (Figure 3). Notably, meta-AAC0005, meta-AAC0007, and meta-AAC0012 also conferred resistance to tobramycin, with the strain harboring meta-AAC0007 demonstrating resistance even at the concentration of 135 μg/mL. On the other hand, no meta-AAC enzyme conferred detectable resistance to kanamycin or amikacin, the 4,5-disubstituted 2-deoxystreptamine aminoglycoside neomycin, or to streptomycin. The strain harboring AAC(3)-Ib demonstrated resistance to gentamicin and sisomicin in accordance with the regiospecificity established for this resistance enzyme.[16] This observed selectivity of the four meta-AAC enzymes for the 4,6-disubstituted 2-deoxystreptamine aminoglycosides is reminiscent of activity established for AAC(3)-I enzymes.[7] At the same time, the ability of meta-AAC0005, meta-AAC0007, and meta-AAC0012 enzymes to confer resistance to tobramycin is in line with AAC(3)-II resistance enzymes.[7] Overall, this analysis showed that meta-AAC enzymes are able to confer high-level resistance to aminoglycosides when heterologously expressed in *E. coli*, on par with the pathogen-originated AAC(3)-Ib.

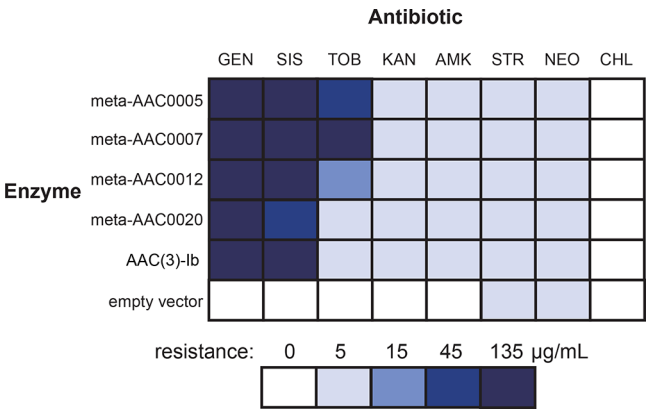

Figure 3. Heterologous aminoglycoside resistance conferred by meta-AAC and AAC(3)-Ib enzymes. As measured by Kirby-Bauer disk diffusion assay in *E. coli* Δ*bamB* Δ*tolC*. Color of each cell corresponds to concentration of aminoglycoside/level of resistance observed, scale at bottom.

***In Vitro* Activity of meta-AAC Enzymes Rivals That of Resistance Enzymes Isolated from Pathogens.** Next, we complemented our *in vivo* data by characterization of the *in vitro* enzymatic properties of meta-AAC enzymes. Each of the four meta-AACs and AAC(3)-Ib was purified, and their activity for gentamicin, sisomicin, or tobramycin substrates was measured in the presence of a saturating concentration of acetyl-CoA (100 μM). Also, the activity of meta-AAC enzymes was measured at varying concentrations of acetyl-CoA (1.25 to 250 μM) in the presence of a saturating concentration of aminoglycoside cosubstrate (gentamicin at 500 μM) . Our obtained data (Table 1) was analyzed using a sigmoidal enzyme activity model, which provided the best fits for all meta-AAC/cosubstrate combinations (sigmoidal and Michaelis−Menten models fits to data are shown in Figure S3). According to this binding model, the Hill coefficients for all four enzymes were greater than 1. Since all four meta-AAC enzymes appear predominantly dimeric in solution as determined by size exclusion chromatography (Figure S2), this was indicative of positive cooperativity between the two subunits in all four meta-AAC enzymes. Selected enzyme−antibiotic pairs demonstrated *H* values greater than 3, particularly meta-AAC0005 and meta-AAC0020; we interpreted this result to indicate a high

Table 1. Steady State Kinetic Parameters for the Wild-Type meta-AAC Proteins and AAC(3)-Ib

		substrate				
enzyme	kinetic parameter	gentamicin	sisomicin	tobramycin	kanamycin	acetyl-CoA
AAC(3)-Ib	$K_{0.5}$ (μM)	35 ± 0.88	28 ± 0.94	24 ± 0.68	456 ± 44.3	18 ± 1.66
	k_{cat} (s^{-1})	0.41 ± 0.005	1.09 ± 0.020	0.22 ± 0.003	0.095 ± 0.005	0.64 ± 0.019
	$k_{cat}/K_{0.5}$ (M^{-1} s^{-1}, ×10^4)	1.1 ± 0.032	3.8 ± 0.14	0.92 ± 0.029	0.021 ± 0.002	3.5 ± 0.33
	H	1.99 ± 0.09	3.28 ± 0.33	2.13 ± 0.13	1.63 ± 0.23	1.80 ± 0.26
meta-AAC0005	$K_{0.5}$ (μM)	26 ± 0.60	8.6 ± 0.22	18.9 ± 0.42	785 ± 58.6	11 ± 0.94
	k_{cat} (s^{-1})	0.16 ± 0.002	0.10 ± 0.00	0.14 ± 0.002	0.186 ± 0.01	0.09 ± 0.003
	$k_{cat}/K_{0.5}$ (M^{-1} s^{-1}, ×10^4)	0.59 ± 0.016	1.1 ± 0.34	0.75 ± 0.20	0.024 ± 0.002	0.80 ± 0.70
	H	4.71 ± 0.52	4.96 ± 0.56	4.15 ± 0.36	2.21 ± 0.06	1.42 ± 0.17
meta-AAC0007	$K_{0.5}$ (μM)	20 ± 1.26	13 ± 0.72	25 ± 3.10	746.8 ± 52.6	16 ± 2.13
	k_{cat} (s^{-1})	0.11 ± 0.002	0.10 ± 0.0022	0.16 ± 0.007	0.187 ± 0.01	0.13 ± 0.005
	$k_{cat}/K_{0.5}$ (M^{-1} s^{-1}, ×10^4)	0.51 ± 0.033	0.78 ± 0.46	0.62 ± 0.80	0.025 ± 0.002	0.75 ± 1.00
	H	1.23 ± 0.07	1.12 ± 0.08	1.07 ± 0.11	2.11 ± 0.2	1.07 ± 0.13
meta-AAC0012	$K_{0.5}$ (μM)	49 ± 1.82	21 ± 2.08	39 ± 1.89	995.5 ± 70.6	22 ± 1.32
	k_{cat} (s^{-1})	0.26 ± 0.005	0.26 ± 0.011	0.38 ± 0.011	0.270 ± 0.02	0.27 ± 0.005
	$k_{cat}/K_{0.5}$ (M^{-1} s^{-1}, ×10^4)	0.52 ± 0.0021	1.2 ± 0.11	0.96 ± 0.054	0.027 ± 0.003	1.2 ± 0.074
	H	1.49 ± 0.06	1.16 ± 0.11	1.68 ± 0.09	3.13 ± 0.5	1.69 ± 0.14
meta-AAC0020	$K_{0.5}$ (μM)	22 ± 0.49	38 ± 1.17	28 ± 1.40	346.4 ± 153	21 ± 1.83
	k_{cat} (s^{-1})	1.17 ± 0.016	2.42 ± 0.049	1.20 ± 0.025	0.207 ± 0.02	1.51 ± 0.045
	$k_{cat}/K_{0.5}$ (M^{-1} s^{-1}, ×10^4)	5.2 ± 0.13	6.4 ± 0.23	4.3 ± 0.44	0.060 ± 0.03	6.9 ± 0.64
	H	3.14 ± 0.22	4.39 ± 0.43	2.30 ± 0.24	0.62 ± 0.07	1.77 ± 0.23

DOI: 10.1021/acsinfecdis.7b00068
ACS Infect. Dis. 2017, 3, 653−665

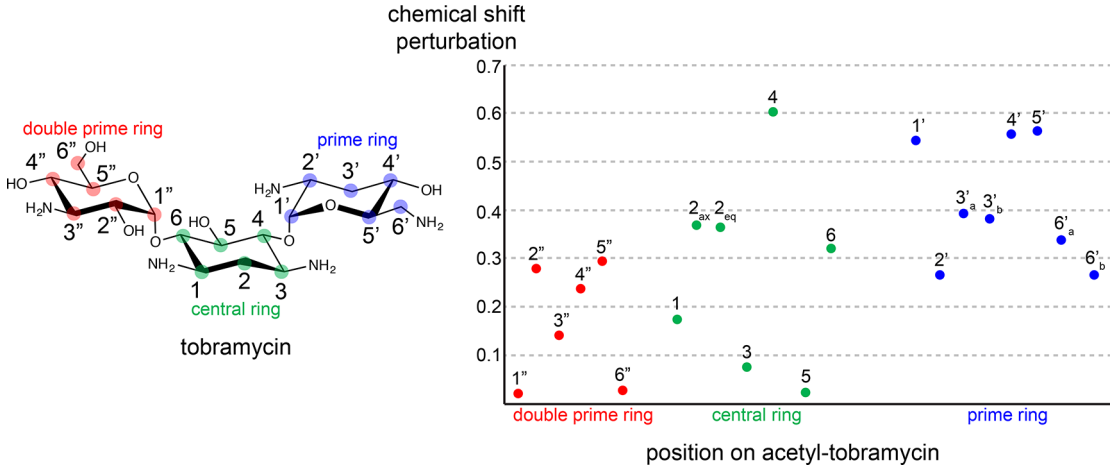

Figure 4. NMR analysis of acetyl-tobramycin. (Left) Chemical structure of tobramycin. Color at each position corresponds to their presence on the double prime, central, or prime rings, respectively. (Right) Chemical shift perturbation values of each position on acetyl-tobramycin relative to unmodified tobramycin, labeled and colored according to chemical structure on the left.

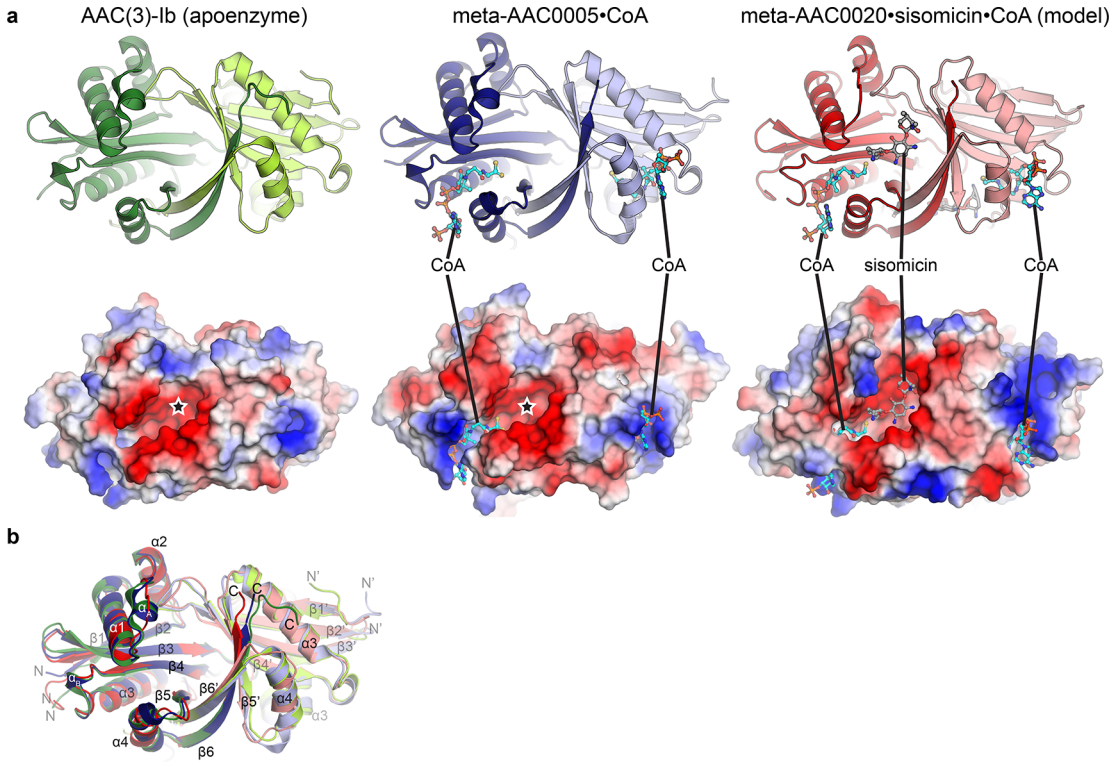

Figure 5. Crystal structures of AAC(3)-Ib, meta-AAC0005−CoA complex and meta-AAC0020−sisomicin−CoA (model from meta-AAC0020^{Y138A}−sisomicin and meta-AAC0020−CoA crystal structures). (a) Top, cartoon representation, with each chain in each dimer colored differently. Bottom, electrostatic surface representations (scale: red = −10 k_B/T, blue = +10 k_B/T, where k_B = Boltzmann's constant). Stars in AAC(3)-Ib and meta-AAC0005 correspond to putative aminoglycoside binding sites. (b) Superposition of structures of AAC(3)-Ib, meta-AAC0005, and meta-AAC0020. Termini and secondary structure elements are labeled.

degree of cooperativity between active sites of this enzyme, an observation previously made for other GNAT family acetyltransferases.[17] Our analysis of the curves did not reveal any evidence of cosubstrate activation or inhibition of meta-AAC enzymes.

The meta-AAC0020 enzyme showed the highest activity in this group, with catalytic efficiency ($k_{cat}/K_{0.5}$) of 4.3−6.4 × 10^4 M^{-1} s^{-1} for the three aminoglycosides substrates (Table 1). The other three meta-AAC enzymes were slightly less active, demonstrating the $k_{cat}/K_{0.5}$ values of 0.5 to 1.1 × 10^4 M^{-1} s^{-1}. The differences in catalytic efficiency between the five tested AAC enzymes was mainly due to differences in substrate turnover (k_{cat}) values, which in the case of the meta-AAC0020 enzyme ranged from 1.2 to 2.4 s^{-1}, while for the other three meta-AAC enzymes and AAC(3)-Ib, this value ranged from 0.10 to 1.1 s^{-1}; the substrate affinity ($K_{0.5}$) values for all five enzymes were in the same range (between 11 and 49 μM) irrespective of cosubstrate. Importantly, the catalytic efficiency of meta-AAC0020 is higher than that of AAC(3)-Ib which demonstrates $k_{cat}/K_{0.5}$ values of 0.9−3.8 × 10^4 M^{-1} s^{-1}. By this

DOI: 10.1021/acsinfecdis.7b00068
ACS Infect. Dis. 2017, 3, 653−665

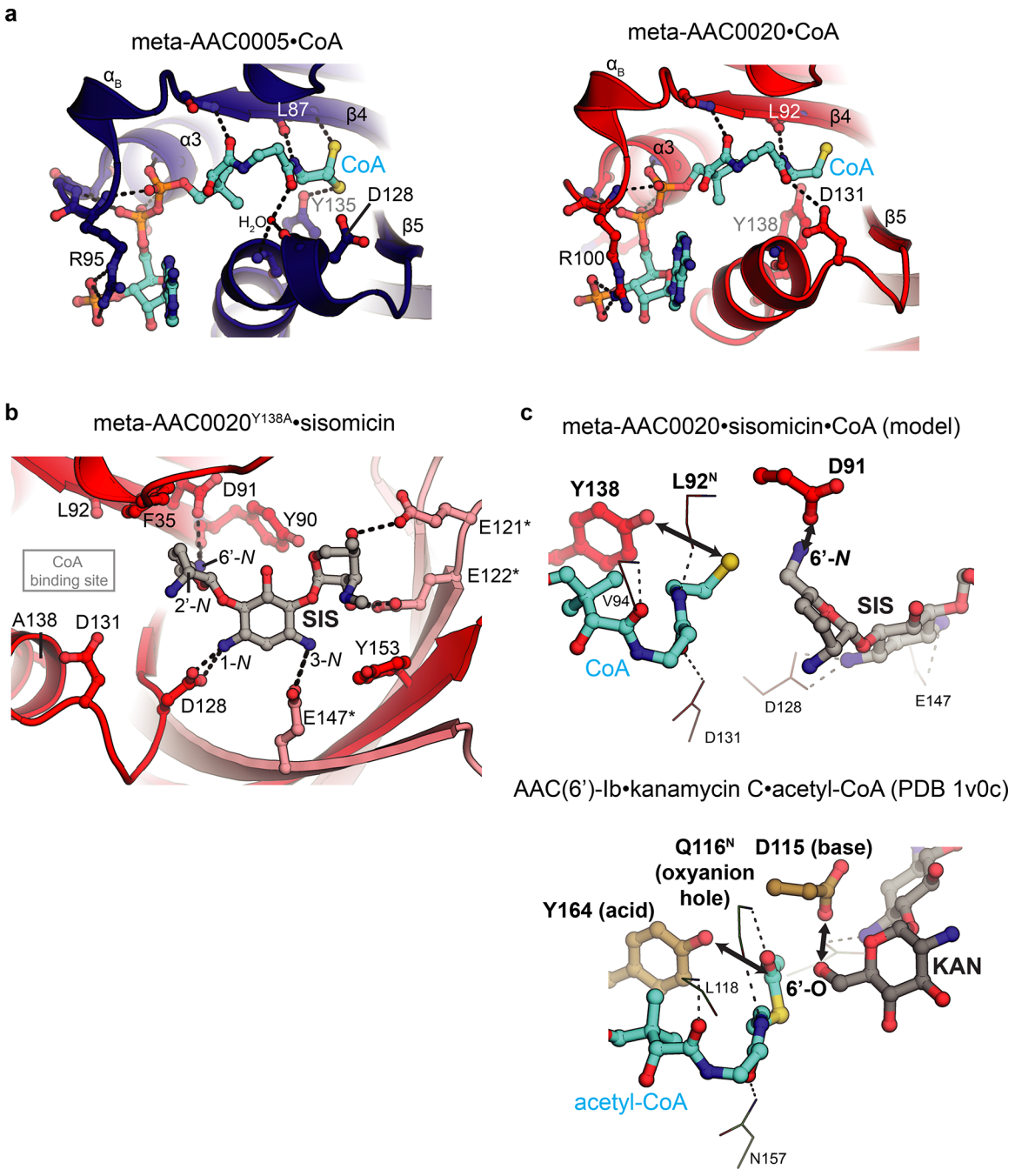

Figure 6. Details of molecular recognition of ligands by meta-AAC0005 and meta-AAC0020. (a) CoA binding site from structure of meta-AAC0005−CoA complex (left) and meta-AAC0020−CoA complex (right). Dashes indicate hydrogen bonds; key residues are labeled; water molecule in meta-AAC0005 active site shown as a red sphere. Asterisks at residue names refer to second chain in dimer. (b) Sisomicin binding site from structure of meta-AAC0020^{Y138A}−sisomicin complex. CoA binding site meta-AAC0020−CoA complex is indicated by a gray box. (c) Comparison of model of meta-AAC0020−sisomicin−CoA complex (constructed by superposition of meta-AAC0020−CoA and meta-AAC0020^{Y138A}−sisomicin complexes) with the crystal structure of AAC(6′)-Ib−kanamycin C−acetyl-CoA complex (PDB 1v0c[19]). Side chains shown in ball-and-stick are the key catalytic residues, while other residues involved in positioning the ligands are shown in thin lines. 6′-substituents of the aminoglycosides are labeled.

in vitro assay, we did not detect activity by any meta-AAC enzyme or AAC(3)-Ib against amikacin or neomycin even with 8× higher concentration of enzyme, but we did detect some activity against kanamycin, although this was much reduced (i.e., for the meta-AAC020 enzyme, the $K_{0.5}$ and k_{cat} parameters for 15- and 6-fold lower). This observation confirmed that the GNAT family meta-AAC enzymes are efficient antibiotic-modifying enzymes comparable to and, in the case of meta-AAC0020, even surpassing the pathogen-isolated AAC(3)-Ib enzyme for acetyltransferase activity.

meta-AAC0020 Mediates Acetylation of the Prime Ring of Aminoglycosides. The superior enzymatic properties of meta-AAC0020 merited further characterization of the activity of this enzyme against aminoglycoside substrates. In order to identify the site-specificity of meta-AAC0020, we undertook analysis of reaction products generated after

DOI: 10.1021/acsinfecdis.7b00068
ACS Infect. Dis. 2017, 3, 653−665

Table 2. X-ray Crystallographic Statistics

enzyme	AAC(3)-Ib	meta-AAC0005·CoA	meta-AAC0020	meta-AAC0020·CoA	meta-AAC0020^{Y138A}·sisomicin
PDB code	4YFJ	5HMN	5F46	5F48	5U08
		Data Collection			
resolution range (Å)	25.0−2.20	20.0−2.02	30.0−1.85	25.0−1.95	19.55−1.52
space group	$P4_12_12$	$P2_12_12_1$	$P2_12_12_1$	$P2_1$	$P1$
a, b, c (Å)	77.0, 77.0, 128.7	58.3, 62.8, 253.6	54.8, 61.8, 114.8	46.1, 80.2, 53.9	46.3, 53.0, 78.7
α, β, γ (deg)	90, 90, 90	90, 90, 90	90, 90, 90	90, 91.97, 90	71.7, 75.6, 88.7
R_{merge} [a]	0.060 (0.694)[b]	0.052 (0.551)	0.032 (0.535)	0.085 (0.611)	0.067 (1.301)
R_{pim} [c]	0.020 (0.238)	0.018 (0.191)	0.013 (0.210)	0.052 (0.370)	0.026 (0.538)
$CC_{1/2}$	0.811[d]	0.903	0.915	0.733	0.799
$\langle I\rangle\sigma I$	3.19 (3.46)	4.10 (4.71)	2.94 (3.63)	3.14 (3.22)	22.3 (2.0)
completeness (%)	95.6 (92.9)	97.2 (97.1)	97.2 (97.1)	97.6 (96.2)	96.6 (93.7)
redundancy	7.9 (8.3)[b]	8.9 (9.0)[b]	6.9 (6.9)[b]	3.6 (3.6)	15.6 (13.3)
		Refinement			
resolution range (Å)	24.36−2.20	19.87−2.02	29.84−1.85	23.62−1.95	19.55−1.52
number of reflections					
working set	18302	62004	31885	27937	100142
test set	916	1995	1592	1403	1999
R_{work}/R_{free} [e]	17.9/23.6	19.1/22.1	20.9/25.3	19.0/23.5	16.6/19.9
number of non-hydrogen atoms, molecules					
protein	2390, 2	7277, 6	2541, 2	2536, 2	5040, 4
co-substrate	N/A	336, 5	N/A	96, 2	124, 4
ion/solvent	35	26	2	4	24
water	242	768	377	420	988
root mean square deviation					
bond length (Å)	0.005	0.016	0.004	0.018	0.015
bond angle (deg)	0.995	1.305	0.781	1.243	1.047
average thermal factor (Å^2)					
protein	45.80	57.66	47.07	31.11	29.2
co-substrate	N/A	250.01	N/A	40.96	67.3
ion/solvent	104.69	79.09	67.47	32.24	30.9
water	50.41	119.48	52.35	43.28	41.8
Ramachandran analysis (%)					
most favored regions	97	96.2	98.3	99	98.7
allowed regions	3	99.8	1.7	1	1.2
disallowed regions	0	0.2	0	0	0

[a] $R_{merge} = \Sigma_{hkl}\Sigma_j|I_{hkl,j} - \langle I_{hkl}\rangle|/\Sigma_{hkl}\Sigma_j I_{hk,j}$, where $I_{hkl,j}$ and $\langle I_{hkl}\rangle$ are the jth and mean measurement of the intensity of reflection j. [b] Values in brackets refer to the highest resolution shells. [c] $R_{pim} = \Sigma_{hkl}\sqrt{(n/n-1)}\ \Sigma_{j=1}^{n}|I_{hkl,j} - \langle I_{hkl}\rangle|/\Sigma_{hkl}\Sigma_j I_{hk,j}$. [d] Value refers to the highest resolution shell. [e] $R = \Sigma|F_p^{obs} - F_p^{calc}|/\Sigma F_p^{obs}$, where F_p^{obs} and F_p^{calc} are the observed and calculated structure factor amplitudes, respectively.

incubation of this enzyme with tobramycin and acetyl-CoA. First, we confirmed the presence of CoA and mono acetyl-tobramycin products in the reaction mixture by LC-MS/MS (Figure S4). Then, we conducted analysis on this reaction mixture by NMR using unmodified tobramycin as a reference.

The heteronuclear ^{1}H-^{13}C HSQC and HMBC and homonuclear TOCSY spectra of the reaction mixture were consistent with those previously reported for AAC enzymatic reaction products,[18] and this allowed for chemical shift assignments and identification of differences between the unmodified and acetylated tobramycin species (see Table S2). In the case of acetyl-tobramycin, we detected chemical shifts corresponding to a single acetyl group (1.91 and 22.45 ppm for ^{1}H and ^{13}C signals, respectively), confirming our mass spectrometry data and demonstrating that the meta-AAC0020 enzyme mediates monoacetylation of this substrate. More importantly, our NMR data shows that the largest chemical shift perturbations (i.e., relative ^{13}C and ^{1}H chemical shifts in tobramycin and acetyl-tobramycin; see Methods) associated with acetylation by the meta-AAC0020 enzyme were localized to the prime ring of the aminoglycoside molecule rather than to the central or the double prime rings (Figure 4). The data (Figure 4) clearly showed that the double prime ring contained the lowest chemical shift perturbations. Accordingly, we postulated that meta-AAC0020 enzyme is either AAC(2′) or AAC(6′) stereospecific rather than AAC(3) as suggested by sequence analysis.

Structural Characterization of meta-AAC0005, meta-AAC0020, and AAC(3)-Ib Demonstrates Significant Structural Similarity in Coenzyme A Binding. We undertook X-ray crystallographic structural characterization of meta-AAC enzymes to provide a molecular framework for our enzymatic analysis. We were successful in determining the structure of the meta-AAC0020 enzyme in apo and CoA-bound forms and meta-AAC0005 in CoA-bound form. We also determined the structure of the AAC(3)-Ib enzyme in apo form. All four structures were solved by Molecular Replacement using the AAC(3)-Ia crystal structure[13] as the search model, and structures were solved to resolutions between 1.52 and 2.20 Å. As we expected, the structures of all three enzymes shared the GNAT fold, with a central six-stranded β-sheet

DOI: 10.1021/acsinfecdis.7b00068
ACS Infect. Dis. 2017, 3, 653−665

following a β1-α1-α2-β2-β3-β4-α3-β5-α4-β6 topology. The three structures superimposed with an average pairwise root-mean-square-deviation (RMSD) value of 0.98 Å, indicating atomic-resolution structural similarity (Figure 5b).

In accordance with our size exclusion chromatography results, the structures of the two meta-AACs and AAC(3)-Ib revealed interdigitated dimers with the β6 strand in each monomer contributing to the central β-sheet in the partner chain. This arrangement resulted in extended dimeric interfaces of approximately 3000 Å^2 in each AAC structure (Figure 5a).

All three AAC structures contained two long clefts (related by the dyad symmetry) divided into a large (approximately 1500 Å^3) negatively charged region and a smaller (approximately 500 Å^3) positively charged region (Figure 5a). The clefts harbored the active site of these enzymes as after structure solution of the meta-AAC0005 and meta-AAC0020 structures we observed additional density corresponding to a single CoA molecule (Figure S5). The position of the CoA molecule in both meta-AAC0005 and meta-AAC0020 structures is very similar, such that the superposition of these two complex structures showed excellent alignment across the bound product molecules except for a difference in the position of the mostly solved-exposed adenine ring (Figure 6a). Furthermore, the interactions between the meta-AAC enzymes and CoA molecules follow characteristics reminiscent of previously characterized GNAT family members.[12] Specifically, a β-bulge formed by β4 residues Tyr85-Asp86 and Tyr91-Asp92 from meta-AAC0005 and meta-AAC0020, respectively, and a $\beta\alpha\beta$ motif (β4-α3-β5) contributed to the pyrophosphate binding site in both complex structures. In both complex structures, backbone amides of the β4-strand formed hydrogen bonds with the pyrophosphate, pantothenate, and β-mercaptoethylamine regions of CoA. As well, the side chain of Arg95/Arg100 in the meta-AAC0005 and meta-AAC0020 enzymes stacked on top of the adenine ring of CoA. Notably, we observed that the side chain conformation of these residues in the CoA-bound structure of meta-AAC0020 is dramatically different compared to the ones in the apo structure of this enzyme, suggesting that these residues may play the role of a molecular "switch" regulating the accessibility of this cosubstrate to the active site.

Despite the overall similarity and conservation of the aforementioned key GNAT superfamily motifs mediating interactions with CoA, we observed nuanced differences in interactions between the two meta-AAC enzymes and CoA molecules. In the meta-AAC0020−CoA complex, the side chain of Asp131 is involved in an interaction with the O5 carbonyl oxygen of the panthothenate group of the substrate molecule, while the interaction between CoA and the equivalent residue in meta-AAC0005 (Asp128) is mediated through a water molecule. Also, the Tyr135 residue in the meta-AAC0005 structure is directly involved in interactions with the sulfhydryl group of CoA, while in meta-AAC0020 structure the equivalent tyrosine residue is at 4.7 Å from the substrate molecule. These differences may underpin the differences in the observed kinetic characteristics of these two enzymes.

Altogether, comparative structural analysis of meta-AACs and AAC(3)-Ib enzymes highlighted the role of specific residues in interactions with CoA. This analysis suggested that these meta-AACs generally follow acetyl-group donor binding in a very similar manner with the other GNAT family members.

meta-AAC0020^{Y138A}−Sisomicin Complex Structure Confirms Its AAC(6′) Regiospecificity. To further characterize the meta-AAC0020 enzyme's activity against aminoglycoside antibiotics, we determined the structure of this enzyme in complex with sisomicin. The interaction between meta-AAC0020 and this compound was stabilized by crystallization of the catalytically inactive mutant Y138A. The asymmetric unit of the meta-AAC0020^{Y138A}−sisomicin complex crystal contained two dimers of this protein (Table 2). The electron density for sisomicin was of the highest quality in one of the two dimers (chains C + D, Figure S5), and this active site was used for detailed analysis of interactions between meta-AAC0020^{Y138A} and sisomicin. The additional electron density detected in the meta-AAC0020^{Y138A} active site allowed us to unambiguously identify the orientation of the central and double prime rings of the aminoglycoside substrate while the position of the prime ring was less clearly defined. As further analysis will show, this observation is likely explained by the extensive hydrogen bonding network between the enzyme and the central and double prime rings of the aminoglycoside that places the prime ring in the closest proximity to the acetyl-CoA cosubstrate, but the absence of acetyl-CoA or CoA in our crystal could explain why the prime ring was less well resolved.

Both chains of the meta-AAC0020 ^{Y138A} dimer contributed to interactions with the aminoglycoside molecule (Figure 6b). More specifically, Asp128 and Glu147 interacted with the central ring 1-amine and 3-amine groups, Glu121 and Glu122 interacted with the 4′′ and 2′′ hydroxyls, and Asp91 interacted with the 6′ amine group. The carbonyl oxygen of Tyr90 also interacted with the 6′ amine. Finally, Tyr153 formed a hydrophobic interaction in the region around the double prime ring and with the backbone of Glu122. Defined by these interactions, the orientation of the sisomicin molecule in the meta-AAC0020^{Y138A} active site placed the amine at 6′ position in proximity to the acetyl-CoA binding pocket and, specifically, to the sulfhydryl group of CoA molecule that we observed in the meta-AAC0020−CoA complex. Thus, the crystal structure clearly indicated that the 6′-amine is the acetylation site for the meta-AAC0020 enzyme.

Taking advantage of the overall structural similarity between the meta-AAC0020^{Y138A}−sisomicin (chain C+D dimer) structure and the meta-AAC0020−CoA structures superimposed (RMSD of 0.27 Å across the dimers), we modeled the ternary complex between meta-AAC0020 and its two cosubstrates. This allowed for further indications of the key catalytic residues in meta-AAC0020. Notably, this model shows excellent spatial conservation with previously characterized AAC(6′)-Ig−kanamycin−acetyl-CoA ternary complex structure (Figure 6c). In this AAC(6′) enzyme, the residues Asp115 and Tyr164 serve as catalytic base and acid, respectively, with Asp115 abstracting a proton from the 6′-amino group (thereby increasing its nucleophilicity for attack on the CoA thioester), and Tyr164 donating a proton to collapse the tetrahedral intermediate.[19] The backbone amide of the Gln116 residue in AAC(6′)-Ib forms an oxyanion hole to stabilize the tetrahedral intermediate.[19] The equivalent residues, Asp91, Tyr90, and Leu92, are conserved in meta-AAC0020 and are positioned in proximity to the 6′-amine.

To validate that these residues are presumptive catalytic determinants, the meta-AAC0020−sisomicin interactions observed in the complex structure were probed by site directed mutagenesis. As was indicated above, the alanine substitution of the Tyr138 residue in contact with the sulfhydryl group of CoA resulted in loss of heterologous resistance in *E. coli* harboring this variant (Figure S6). Alanine substitution of Asp91, the

DOI: 10.1021/acsinfecdis.7b00068
ACS Infect. Dis. 2017, 3, 653−665

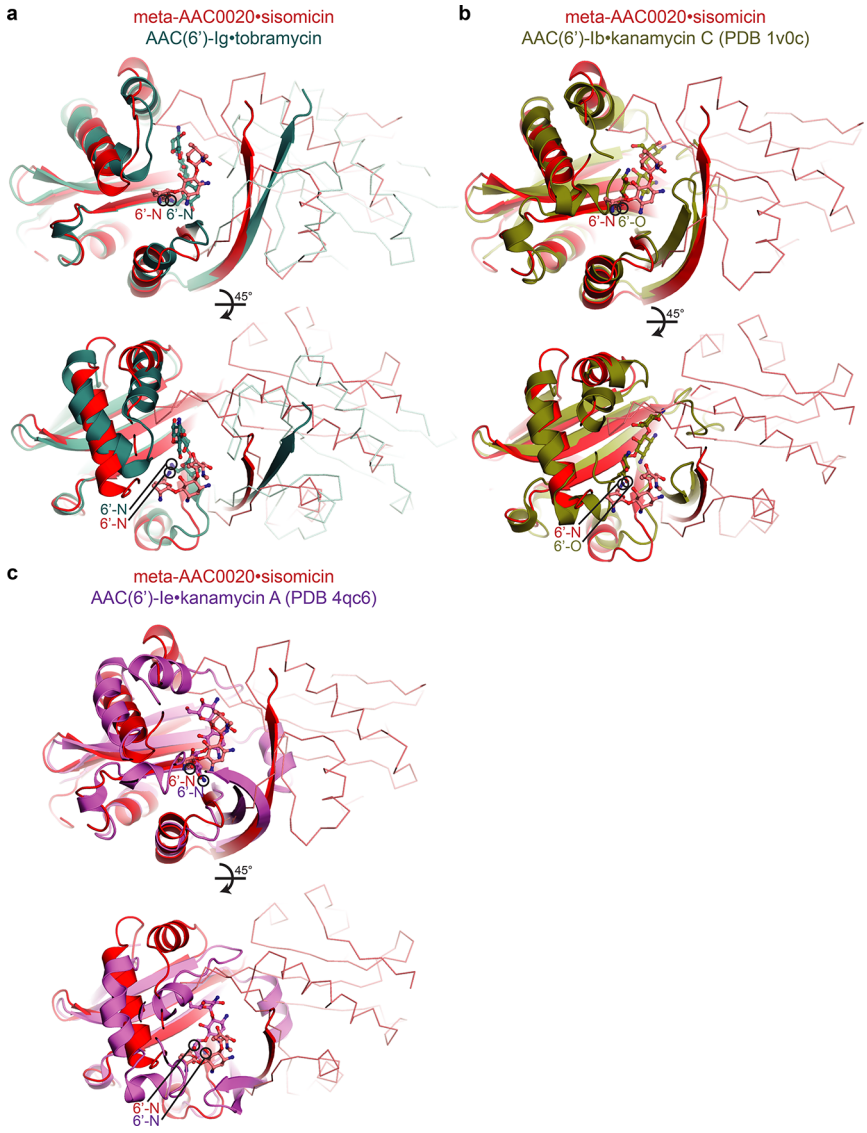

Figure 7. Comparison of structures of meta-AAC0020^{Y138A}–sisomicin with AAC(6′)-Ig–tobramycin, AAC(6′)-Ib–kanamycin C, and AAC(6′)-Ie–kanamycin A. (a) Superposition of meta-AAC0020^{Y138A}–sisomicin and AAC(6′)-Ig–tobramycin complexes. (b) Superposition of meta-AAC0020^{Y138A}–sisomicin and AAC(6′)-Ib–kanamycin C complexes. (c) Superposition of meta-AAC0020^{Y138A}–sisomicin and AAC(6′)-Ie–kanamycin A complexes. Bound aminoglycosides are shown with ball-and-stick representation, and 6′ substituents are circled and labeled.

residue that interacted with the 6′ amine group, also resulted in complete loss of resistance. Likewise, the Leu92Pro substitution, designed to abrogate the backbone amide interactions with the cosubstrate's sulfhydryl group, also compromised the resistance of the corresponding *E. coli* strain. Finally, the Asp131Ala mutation affecting interaction with the oxygen of the pantothenate region of CoA resulted in significant decrease in resistance (Figure S6). This meta-AAC0020 variant was also severely compromised for acetylation activity, demonstrating 3- to 40-fold lower $k_{cat}/K_{0.5}$ values against the four tested aminoglycosides (Figure S6). Overall, these results validate that the residues identified in the crystal structure of meta-AAC0020^{Y138A} in complex with sisomicin play key roles in catalysis by this enzyme, consistent with our data identifying this enzyme as a new member of the AAC(6′) regiospecificity group.

meta-AAC0020 Is a AAC(6′) Enzyme Demonstrating a Novel Drug Recognition Mode. Given that its crystal structure, NMR analysis, and mutagenesis identified that meta-AAC0020 possesses catalytic specificity for the 6′-amine, we were interested in a structural comparison with other characterized AAC(6′) enzymes. The crystal structures of the meta-AAC0020 and AAC(6′)-Ig enzymes shared the most overall structural similarity with RMSD of 2.2 Å across matching Cα atoms, and their dimerization modes were very similar (Figure 7a). However, the position of the bound aminoglycosides in the meta-AAC0020–sisomicin and AAC(6′)-Ig–tobramycin complexes are quite distinct, except for the position of the 6′-amine groups targeted for acetylation. Overall, the aminoglycoside molecule appears much deeper immersed in the active site of AAC(6′)-Ig than in that of meta-AAC0020. A comparison of the meta-AAC0020–sisomicin complex with AAC(6′)-Ie–kanamycin and AAC(6′)-Ib–kanamycin structures reiterated this observation: a single chain of the meta-AAC0020 dimer is readily aligned with the single chains of both AAC(6′)-Ib (Figure 7b) and AAC(6′)-Ie (Figure 7c), despite that the latter two enzymes are predominantly monomeric. Similar to the comparison

DOI: 10.1021/acsinfecdis.7b00068
ACS Infect. Dis. 2017, 3, 653–665

described above, the position of the 6′ substituents of the enzyme-bound aminoglycosides aligned well, but the remainder of the drugs did not. The drugs were much more deeply localized into the active sites of AAC(6′)-Ib and AAC(6′)-Ie (i.e., larger buried surface area of each compound by interactions with these two enzymes, respectively) than in that of meta-AAC0020. In addition, the interactions we observed between meta-AAC0020 and sisomicin were not conserved in AAC(6′)-Ib and -Ie. Overall, this analysis showed that, while meta-AAC0020 harbors AAC(6′) activity and places the acetylation site of sisomicin at a spatially conserved position with AAC(6′) enzymes, it possesses distinct molecular binding determinants to recognize the other parts of the 4,6′-disubstituted aminoglycoside scaffold.

DISCUSSION

The rise of resistance to aminoglycoside antibiotics in the clinic is associated primarily with the activity of aminoglycoside modifying enzymes, of which AACs are of particular relevance. The search for the origin of these and other classes of resistance enzymes pointed to the environmental microbiome as a vast reservoir of proto-resistance genes. Accordingly, a detailed analysis of the environmental resistome is required in order to understand and anticipate the inevitable emergence of novel forms of resistance in human pathogens. Here, we present the detailed functional and structural analysis of four AACs isolated from the environmental microbiome. These enzymes demonstrate very similar enzymatic properties, and the properties of the meta-AAC0020 enzyme exceed those of AAC enzymes isolated from pathogens.

For our analysis, we selected meta-AAC sequences sharing substantial sequence similarity with AAC enzymes isolated from human pathogens, enabling direct comparative analysis. For example, meta-AAC0005 is 67% identical to AAC(3)-Ia and -Ib suggesting possible common ancestry between these enzymes. Moreover, through crystallographic analysis, we demonstrated that sequence similarity between meta-AACs and the clinically sourced AAC(3)-Ia and AAC(3)-Ib is reflected in their 3D structures, which share the overall fold typical of the GNAT family. However, through combination of structural and enzymatic studies, we demonstrate that, rather than the expected AAC(3) regiospecificity as suggested by the sequence similarity, meta-AAC0020 actually possesses AAC(6′) specificity. Analysis of meta-AAC0020−sisomicin and meta-AAC0020−CoA complex structures pointed to specific residues involved in orientation of the 6′-amine of the aminoglycoside substrate and the sulfhydryl group of CoA, providing novel insight into interactions between AAC enzymes and their substrates. Not only is meta-AAC0020 a novel AAC(6′) enzyme, but also the precise spatial orientation of sisomicin in the meta-AAC0020 active site is different than that in previously characterized clinical AAC(6′) enzymes. Thus, our study of proto-resistome enzymes identifies a novel substrate recognition mode and reveals previously unknown diversity among AAC(6′) enzymes. These results raise questions about the details of the substrate recognition mode of clinical AAC(3)-I enzymes, which have not yet been structurally characterized in complex with aminoglycosides; it is possible some of these are actually AAC(6′) enzymes.

Analysis of the meta-AAC0020^{Y138A}−sisomicin crystal structure also provided a possible explanation of this enzyme's aminoglycoside specificity. According to our resistance assays, meta-AAC0020 is ineffective against amikacin, which possesses a hydroxyl group at the 3′ position. The meta-AAC0020 enzyme was able to modify kanamycin which also possesses this hydroxyl group, but the activity was much reduced. Modeling of these aminoglycosides onto the meta-AAC0020^{Y138A}−sisomicin structure suggests that the 3′ hydroxyl would clash with Phe35 of the enzyme. Similarly, modeling of amikacin suggests its 1-*N*-2-hydroxybutyrlamine substituent would clash with Asp128 from β5 of meta-AAC0020, and the combination of this substituent and the 3′ hydroxyl would abrogate activity by meta-AAC020. meta-AAC0020 is also ineffective against neomycin; since the meta-AAC0020^{Y138A}−sisomicin structure indicates that the sisomicin double prime ring forms many interactions with the enzyme, neomycin lacks this interaction as it lacks this ring. Finally, streptomycin lacks the core features of the 4,6-disubstutited aminoglycosides and as such can not be modified by the meta-AAC0020 enzyme.

The meta-AAC enzymes were ineffective against certain classes of aminoglycoside antibiotics represented by kanamycin A and amikacin. Our structural analysis identified that the specific AAC active site architectural details were incompatible with the recognition of these particular aminoglycosides. Such detailed analysis is important for the design of novel aminoglycoside antibiotics less prone to modification by AAC enzymes and less prone to novel AACs in the environment. For example, modification of the prime ring of an aminoglycoside to include a substituent at the 3-position would introduce a steric clash with the meta-AAC0020 residue Phe35 and would be expected to block the activity of this enzyme; all of the preferred substrates, sisomicin, tobramycin, and gentamicin, do not contain a substituent at this position. Another possibility is modification of the 2′′-OH group to block its interaction with the meta-AAC0020 residue Glu122.

Interestingly, a homologue of the meta-AAC0020 enzyme (65% identical in sequence) could be identified in *Elizabethkingia anophelis* by a BLAST search of the NCBI database (accession WP_024568394.1). This putative AAC gene is found in a genetic environment next to an integrase gene. This is consistent with the notion that environmental AAC genes are reservoirs for the transmission to human pathogens and illustrates that a homologue of the *meta-AAC0020* gene has already transferred to a pathogen; perhaps this has or will arise in a clinical setting to cause aminoglycoside resistance.

In conclusion, this study showed that AAC enzymes of environmental origin possess acetylation activity that rivals those of their mobilized counterparts in pathogens and can provide insights into previously unknown modes of antibiotic recognition. Overall, our findings provide molecular details of the richness, diversity, and complexity of the environmental resistome that if mobilized into pathogens could provide new types of clinical antibiotic resistance and further show the difficult and daunting task of overcoming the antibiotic crisis.

METHODS

Antibiotics. Kanamycin A (KAN), amikacin (AMI), tobramycin (TOB), gentamicin (GEN, mixture of C_1, C_{1a}, and C_2 forms), sisomicin (SIS), neomycin (NEO, ≥85% neomycin B with the remainder as neomycin C), streptomycin (STR), and chloramphenicol (CHL) were purchased from Sigma-Aldrich or Bioshop. Amikacin (AMI) was purchased from Alfa Aesar.

Phylogenetic Analysis. AAC(3) representative sequences chosen for analysis included AAC(3)-I, AAC(3)-II, AAC(3)-III, AAC(3)-IV, AAC(3)-VI, AAC(3)-VII, AAC(3)-VIII, AAC(3)-

DOI: 10.1021/acsinfecdis.7b00068
ACS Infect. Dis. 2017, 3, 653−665

IX, and AAC(3)-X. As AAC(3)-V has been reported to confer resistance to the same aminoglycosides as AAC(3)-II, only AAC(3)-II was included in our analysis. Sequence alignment was performed using the Clustal Omega server (EMBL-EBI). The phylogenetic tree was generated by MrBayes,[20] and the phylogenetic trees were visualized using FigTree.

Cloning and Protein Purification. cDNA for *aac(3)-Ib* was cloned into the vector pNIC-CH, coding for a fusion protein with a noncleavable C-terminal His_6-tag. cDNA coding for each of the *meta-aac0005*, *meta-aac0007*, *meta-aac00012*, and *meta-aac0020* genes was cloned into the pMCSG53 vector,[21] coding for fusion proteins with a N-terminal His_6-tag followed by a TEV protease cleavage site. The meta-AAC0020 site-directed mutants L92P, Y138A, D91A, and D131A were prepared using a method modified from the QuickChange site-directed mutagenesis protocol (Stratagene, La Jolla, CA).

E. coli BL21(DE3)-RIL competent cells were transformed with the pNIC-CH plasmid while *E. coli* BL21(DE3)-Gold cells were transformed with the pMCSG53 plasmids. Three mL of overnight culture was diluted into 1 L of LB media containing selected antibiotics (chloramphenicol and kanamycin for AAC(3)-Ib, ampicillin for meta-AAC enzymes) and grown at 37 °C with shaking. Expression was induced with IPTG at 17 °C when OD_{600} reached 0.6−0.8. The large overnight cell culture was then collected by centrifugation at 7000*g*. Ni-NTA affinity chromatography was used for protein purification. Cells were resuspended in binding buffer [pH 7.5, 100 mM HEPES, 500 mM NaCl, 5 mM imidazole, and 5% glycerol (v/v)] and lysed with a sonicator, and cell debris was removed by centrifugation at 30 000*g*. The cell lysate was loaded on a 4 mL Ni-NTA column (QIAGEN) pre-equilibrated with 250 mL of binding buffer and washed with wash buffer [pH 7.5, 100 mM HEPES, 500 mM NaCl, 30 mM imidazole, and 5% glycerol (v/v)], and the proteins were eluted with elution buffer [pH 7.5, 100 mM HEPES, 500 mM NaCl, 250 mM imidazole, and 5% glycerol (v/v)]. The meta-AAC-His_6-tagged proteins were then subjected to overnight TEV cleavage using 50 μg of TEV protease per mg of His_6-tagged protein in binding buffer and dialyzed overnight against the binding buffer. The His_6-tag and TEV was removed by running the protein again over the Ni-NTA column. The tag-free proteins and AAC(3)-Ib with retained C-terminal His_6 tag were dialyzed in pH 7.5, 50 mM HEPES with 500 mM NaCl overnight, and the purity of the protein was analyzed by SDS-polyacrylamide gel electrophoresis. The purified proteins were also subjected to size exclusion chromatography (Superdex 200 10/300GL) analysis for determination of their oligomeric state, using the same final buffer as noted above.

Heterologous Aminoglycoside Resistance Test (Kirby Bauer Disk Diffusion Assay). The full-length wild-type and/or mutants of AAC(3)-Ib, meta-AAC0005, meta-AAC0007, and meta-AAC0020 were cloned into the pUC18 expression vector. The hyperpermeable mutant strain of *E. coli* (Δ*tolC* Δ*bamB*) was received as a gift from Prof. Gerard D. Wright, McMaster University. Three mL overnight cultures of this strain were diluted 1:50 into fresh LB medium, containing 100 μg/mL ampicillin. The cell cultures were then incubated at 37 °C until the midexponential phase (OD_{600} 0.7−0.8). The cells were spread onto LB agar plates using a sterile swab. The LB agar plates were prepared to contain 100 μg/mL selection antibiotic ampicillin, and then, 100 μL of fresh 0.1 M IPTG was applied. Sterile paper disks were soaked with LB medium and aminoglycoside antibiotics at various concentrations (5, 15, 45, and 135 μg/mL) and placed on top of the plates. The plates were incubated overnight at 37 °C, and the next day plates were visually inspected: resistance was assigned if no zone of killing by antibiotic was observed. *E. coli* transformed with empty vector or meta-AAC carrying *E. coli* plated on 5 μg/mL chloramphenicol was used as the positive control.

Aminoglycoside N-Acetyltransferase Activity Assay. Aminoglycoside *N*-acetyltransferase activity was monitored spectrophotometrically by following the increase in absorbance at 324 nm based on the reaction between the acetylation reaction product CoASH and 4,4′-dipyridyldisulfide, releasing 4-thiopyridone ($\varepsilon_{324\ nm}$ = 19 800 M^{-1} cm^{-1}). Reactions were performed in 96-well plate format as triplicates at 25 °C. Each assay reaction was conducted by adding 180 μL of assay mixture (50 mM Acetyl CoA, 100 mM 4,4′-dipyridyldisulfide, pH 7.5, 500 mM Tris-HCl, and 125 mM EDTA) to 10 μL of protein stock solution (0.05−0.4 mg/mL). Reactions were initiated by adding 10 μL of aminoglycoside. The initial velocity pattern was obtained at a range of gentamicin (0.5−500 μM), sisomicin (2.5−500 μM), and tobramycin (0.5−500 μM) with six different concentrations of acetyl-CoA (5, 10, 25, 100, 150, and 250 μM). Absorbance values at 324 nm were monitored on a Spectra Max M2 microplate reader every 30 s for a total time of 10 min. Kinetic parameters were determined by nonlinear curve fitting into the equation below, using GraphPad Prism 4.0 software (GraphPad Software, U.S.).

$$v = (V_m[A]^h)/(K^h + [A]^h)$$

where v is the initial velocity, V_m is the maximal velocity, $[A]$ is the concentration of substrate, $K_{0.5}$ is the substrate concentration at half maximal velocity, and h is the Hill coefficient.

NMR Analysis. Since a commercially available tobramycin sample contained higher purity (≥98% by TLC) compared to sisomicin (≥80% by TLC) and gentamicin (only available as a mixture of gentamicin C_1, C_{1a}, and C_2 isoforms), the NMR analysis was only performed on tobramycin. Tobramycin solution (250 μL) was prepared from powder (7.5 mg) using $NaHPO_4$ (pH 6.75, 50 mM) and D_2O (>90%). The acetylation reaction sample was prepared by incubating the reaction of Na_2HPO_4 (50 mM, pH 7.0), tobramycin (30 mM), meta-AAC0020 enzyme (0.05 mg/mL), and acetyl-CoA (30 mM) for 24 h at 4 °C. NMR spectra of tobramycin substrate and acetylated tobramycin were collected at 298 K on a Bruker AV3 system operating at 600 MHz and equipped with a cryogenic probe. Standard heteronuclear ^1H-^{13}C HSQC and HMBC spectra were acquired with 200−256 indirect points in the carbon dimension over sweep widths of 120 and 240 ppm, respectively. Homonuclear TOCSY spectra were collected with 256 indirect points and sweep widths of 10 ppm in both the direct and indirect dimensions. All spectra were processed and analyzed using the software Topspin (Bruker Biospin). Δppm was calculated using the equation below:

Δppm = ^1H or ^{13}C chemical shift of acetylated tobramycin − ^1H or ^{13}C chemical shift of acetylated tobramycin product.

The chemical shift perturbation (CSP) values of each position on the acetyl-tobramycin molecule relative to unmodified tobramycin were calculated using the equation below, where 5.9 is a factor to account differences in chemical shift dispersion between ^1H and ^{13}C.

$$CSP = \sqrt{\frac{\Delta ppm\ of\ ^{13}C^2}{5.9} + (\Delta ppm\ of\ ^1H)^2}$$

DOI: 10.1021/acsinfecdis.7b00068
ACS Infect. Dis. 2017, 3, 653−665

LC-MS/MS Analysis of Tobramycin and Acetyl-Tobramycin. Tobramycin (15 mM) was incubated in a reaction buffer of ammonium bicarbonate (pH 8.0, 15 mM), acetyl-CoA (20 mM), and either meta-AAC0020, AAC(6′)-Ig, or AAC(2′)-Ia (0.05 mg/mL) for 24 h at 4 °C. Protein was filtered out using centrifugal MWCO filters (10 kDa, Nanosep) prior to analysis. Five μL of the reaction products was injected onto a Dionex Ultimate 3000 UHPLC system equipped with a Luna NH2 column (150 × 2 mm, 3 μm particle size, Phenomenex, U.S.). Chromatography was performed at a flow rate of 200 $\mu L \cdot min^{-1}$ with the following gradient: 0−1 min, 98% mobile phase A (0.1% formic acid in acetonitrile); 1−15 min, gradient to 98% mobile phase B (0.1% formic acid in water); 15−20 min, 98% B; this was followed by re-equilibration of the column at 98% A for 5 min. Detection of reaction products was performed using a Q-Exactive mass spectrometer equipped with a HESI source (Thermo Scientific) running a "Top 5" data dependent aquisition method in positive ionization mode, with an MS1 precursor scan range of 50−750 m/z, resolution of 70 000, AGC target of 3×10^6, and a maximum injection time (IT) of 100 ms. For each MS1 scan, the top 5 most intense ions were selected for HCD at a normalized collision energy of 20, an isolation window of 2 m/z, 17 500 resolution, AGC target of 1×10^5, and max IT of 150 ms. A dynamic exclusion window of 10 s was set to avoid repeat analysis of the same precursor ions.

Retention times were aligned to a tobramycin reference standard, and extracted ion chromatograms (EIC) and MS/MS spectra for both tobramycin (m/z values: $[M + 3H]^{+3}$ = 156.75, $[M + 2H]^{+2}$ = 234.63, $[M + H]^{+}$ = 468.26) and monoacetylated tobramycin (m/z values: $[M + 3H]^{+3}$ = 170.76, $[M + 2H]^{+2}$ = 255.64, $[M + H]^{+}$ = 510.27) were prepared using Xcalibur. No spectra corresponding to doubly acetylated tobramycin ($[M + H]^{+}$= 552.27) were detectable.

Crystallization and Structure Determination. All crystals were grown at room temperature using the vapor diffusion sitting drop method with 0.5 μL of protein solution mixed with 0.5 μL of reservoir solution. Apoenzyme AAC(3)-Ib (at 10 mg/mL protein) was crystallized in a solution containing 40% (w/v) PEG 300 and phosphate-citrate (pH 5.2). The CoA-bound complex of meta-AAC0005 (at 20 mg/mL protein) was cocrystallized from a solution containing 25% (w/v) PEG 3350, 0.2 M magnesium formate in the presence of 10 mM sisomicin. Apoenzyme meta-AAC0020 (at 20 mg/mL protein) was crystallized in a solution containing 4 M sodium formate. CoA-bound meta-AAC0020 (at 20 mg/mL protein) was cocrystallized from the same solution in the presence of 20 mM gentamicin and 20 mM acetyl-CoA. The meta-$AAC0020^{Y138A}$−sisomicin complex was crystallized with 10 mg/mL protein, using crystal seeds grown in a solution containing 20% (w/v) PEG3350, 0.2 M calcium acetate, and 20 mM sisomicin for 48 h, and crystals were then subject to soaking with an additional 20 mM sisomicin for another 24 h. Crystals were cryoprotected with Paratone-N prior to flash-freezing in liquid nitrogen prior to diffraction data collection. Diffraction data was processed by HKL3000[22] for all structures except for the meta-$AAC0020^{Y138A}$−sisomicin complex which was processed by XDS[23] and Aimless.[24] All structures were solved by Molecular Replacement using the structures of AAC(3)-Ia,[13] AAC(3)-Ib, or meta-AAC0020 and Phenix.phaser.[25] Structure refinement was performed using Phenix.refine plus manual building with Coot.[26] The presence of cosubstrate molecules was identified by building into the $F_o - F_c$ difference density after the initial rounds of refinement; occupancy of sisomicin molecules was refined. For all structures, B-factors were refined as anisotropic for protein atoms and isotropic for nonprotein atoms and TLS parametrization was included in the refinement. Average B-factor and bond angle/length RMSD values were calculated using Phenix. All geometry was verified using the Phenix, Coot, and wwPDB validation tools. All structures were deposited in the Protein Databank (accession codes listed in Table 2).

Structural Analysis. Electrostatic surfaces were produced using PyMol.[27] Dimerization interface burial was determined by PDBePISA.[28] Active site cleft volumes were determined by the CastP server.[29] Protein−ligand interactions were determined by Coot and PyMol.

■ ASSOCIATED CONTENT

Supporting Information

The Supporting Information is available free of charge on the ACS Publications website at DOI: 10.1021/acsinfecdis.7b00068.

Contains alignment of GNAT and Antibiotic_NAT family AAC and meta-AAC enzyme sequences; size exclusion chromatography profiles of purified enzymes; kinetics data with fits to models; LC-MS/MC profiles of tobramycin and acetyl-tobramycin products of meta-AAC0020-catalyzed reaction; electron density and details of coenzyme A and sisomicin binding to meta-AAC crystal structures; disk diffusion and kinetics analysis of meta-AAC0020 mutant enzymes; table of meta-AAC orthologs via BLAST searches; table of NMR chemical shifts of tobramycin and acetyl-tobramycin products of meta-AAC0020-catalyzed reaction (PDF)

■ AUTHOR INFORMATION

Corresponding Author

*Tel: +1-403-210-7980. E-mail: alexei.savchenko@ucalgary.ca.

ORCID

Alexei Savchenko: 0000-0002-5256-9237

Present Address

◆K.J.F.: Basic Sciences Division, Fred Hutchinson Cancer Research Center, P.O. Box 19024, Seattle, WA, USA, 98109-1024.

Notes

The authors declare no competing financial interest.

■ ACKNOWLEDGMENTS

This project has been funded in whole or in part with Federal funds from the National Institute of Allergy and Infectious Diseases, National Institutes of Health (NIH), Department of Health and Human Services, under Contract No. HHSN272201200026C. This work was also supported in part by an award to G.D. through the NIH Director's New Innovator Award (DP2-DK-098089). K.J.F. received support from the NIGMS Cell and Molecular Biology Training Grant (GM 007067), the NHGRI Genome Analysis Training Program (T32 HG000045), and the NSF as a graduate research fellow (award number DGE-1143954). The content is solely the responsibility of the authors and does not necessarily represent the official views of the funding agencies. We thank Drs. Darcy Burns and Sergiy Nokhrin for initial NMR studies

DOI: 10.1021/acsinfecdis.7b00068
ACS Infect. Dis. 2017, 3, 653−665

and Robert Flick for helpful discussions on kinetics. *E. coli* (Δ*bamB* Δ*tolC*) strain was a gift from Gerry Wright.

REFERENCES

(1) Forsberg, K. J., Patel, S., Gibson, M. K., Lauber, C. L., Knight, R., Fierer, N., and Dantas, G. (2014) Bacterial phylogeny structures soil resistomes across habitats. *Nature 509*, 612−616.
(2) World Health Organization (WHO). (2014) *Antimicrobial resistance: global report on surveillance*, WHO, Geneva.
(3) Pehrsson, E. C., Forsberg, K. J., Gibson, M. K., Ahmadi, S., and Dantas, G. (2013) Novel resistance functions uncovered using functional metagenomic investigations of resistance reservoirs. *Front. Microbiol. 4*, 145.
(4) von Wintersdorff, C. J. H., Penders, J., van Niekerk, J. M., Mills, N. D., Majumder, S., van Alphen, L. B., Savelkoul, P. H. M., and Wolffs, P. F. G. (2016) Dissemination of Antimicrobial Resistance in Microbial Ecosystems through Horizontal Gene Transfer. *Front. Microbiol. 7* (110), 173.
(5) Waksman, S. A., Bugie, E., and Schatz, A. (1944) Isolation of Antibiotic Substances from Soil Micro-Organisms, with special reference to Streptothricin and Streptomycin. *Proc. Staff Meet. Mayo Clin. 19*, 537−548.
(6) Poulikakos, P., and Falagas, M. E. (2013) Aminoglycoside therapy in infectious diseases. *Expert Opin. Pharmacother. 14* (12), 1585−1597.
(7) Becker, B., and Cooper, M. A. (2013) Aminoglycoside antibiotics in the 21st century. *ACS Chem. Biol. 8* (1), 105−115.
(8) Ramirez, M. S., and Tolmasky, M. E. (2010) Aminoglycoside modifying enzymes. *Drug Resist. Updates 13* (6), 151−171.
(9) Costa, Y., Galimand, M., Leclercq, R., Duval, J., and Courvalin, P. (1993) Characterization of the chromosomal *aac(6′)-Ii* gene specific for *Enterococcus faecium*. *Antimicrob. Agents Chemother. 37* (9), 1896−1903.
(10) Stogios, P. J., Kuhn, M. L., Evdokimova, E., Law, M., Courvalin, P., and Savchenko, A. (2017) Structural and biochemical characterization of Acinetobacter spp. aminoglycoside acetyltransferases highlights functional and evolutionary variation among antibiotic resistance enzymes. *ACS Infect. Dis. 3*, 132.
(11) Magnet, S., Lambert, T., Courvalin, P., and Blanchard, J. S. (2001) Kinetic and mutagenic characterization of the chromosomally encoded *Salmonella enterica* AAC(6′)-Iy aminoglycoside N-acetyltransferase. *Biochemistry 40* (12), 3700−3709.
(12) Favrot, L., Blanchard, J. S., and Vergnolle, O. (2016) Bacterial GCN5-Related N-Acetyltransferases: From Resistance to Regulation. *Biochemistry 55* (7), 989−1002.
(13) Wolf, E., Vassilev, A., Makino, Y., Sali, A., Nakatani, Y., and Burley, S. K. (1998) Crystal structure of a GCN5-related N-acetyltransferase: Serratia marcescens aminoglycoside 3-N-acetyltransferase. *Cell 94* (4), 439−449.
(14) Stogios, P. J., Spanogiannopoulos, P., Evdokimova, E., Egorova, O., Shakya, T., Todorovic, N., Capretta, A., Wright, G. D., and Savchenko, A. (2013) Structure-guided optimization of protein kinase inhibitors reverses aminoglycoside antibiotic resistance. *Biochem. J. 454* (2), 191−200.
(15) Bauer, A. W., Kirby, W. M., Sherris, J. C., and Turck, M. (1966) Antibiotic susceptibility testing by a standardized single disk method. *Am. J. Clin. Pathol. 45* (4), 493−496.
(16) Schwocho, L. R., Schaffner, C. P., Miller, G. H., Hare, R. S., and Shaw, K. J. (1995) Cloning and characterization of a 3-N-aminoglycoside acetyltransferase gene, aac(3)-Ib, from Pseudomonas aeruginosa. *Antimicrob. Agents Chemother. 39* (8), 1790−1796.
(17) Tang, Y., Holbert, M. A., Wurtele, H., Meeth, K., Rocha, W., Gharib, M., Jiang, E., Thibault, P., Verreault, A., Cole, P. A., Marmorstein, R., et al. (2008) Fungal Rtt109 histone acetyltransferase is an unexpected structural homolog of metazoan p300/CBP. *Nat. Struct. Mol. Biol. 15* (7), 738−745.
(18) Eneva, G. I., Spassov, S. L., and Haimova, M. A. (1995) Complete 1H and 13C NMR Chemical Shift Assignments for Some N-Polyformylated Aminoglycoside Antibiotics. *Spectrosc. Lett. 28* (1), 69−79.
(19) Vetting, M. W., Park, C. H., Hegde, S. S., Jacoby, G. A., Hooper, D. C., and Blanchard, J. S. (2008) Mechanistic and structural analysis of aminoglycoside N-acetyltransferase AAC(6“)-Ib and its bifunctional, fluoroquinolone-active AAC(6”)-Ib-cr variant. *Biochemistry 47* (37), 9825−9835.
(20) Ronquist, F., and Huelsenbeck, J. P. (2003) MrBayes 3: Bayesian phylogenetic inference under mixed models. *Bioinformatics 19* (12), 1572−1574.
(21) Eschenfeldt, W. H., Makowska-Grzyska, M., Stols, L., Donnelly, M. I., Jedrzejczak, R., and Joachimiak, A. (2013) New LIC vectors for production of proteins from genes containing rare codons. *J. Struct. Funct. Genomics 14* (4), 135−144.
(22) Minor, W., Cymborowski, M., Otwinowski, Z., and Chruszcz, M. (2006) HKL-3000: the integration of data reduction and structure solution–from diffraction images to an initial model in minutes. *Acta Crystallogr., Sect. D: Biol. Crystallogr. 62* (8), 859−866.
(23) Kabsch, W. (2010) XDS. *Acta Crystallogr., Sect. D: Biol. Crystallogr. 66* (2), 125−132.
(24) Winn, M. D., Ballard, C. C., Cowtan, K. D., Dodson, E. J., Emsley, P., Evans, P. R., Keegan, R. M., Krissinel, E. B., Leslie, A. G. W., McCoy, A., et al. (2011) Overview of the CCP4 suite and current developments. *Acta Crystallogr., Sect. D: Biol. Crystallogr. 67* (4), 235−242.
(25) Adams, P. D., Afonine, P. V., Bunkóczi, G., Chen, V. B., Davis, I. W., Echols, N., Headd, J. J., Hung, L. W., Kapral, G. J., Grosse-Kunstleve, R. W., et al. (2010) PHENIX: a comprehensive Python-based system for macromolecular structure solution. *Acta Crystallogr., Sect. D: Biol. Crystallogr. 66* (2), 213−221.
(26) Emsley, P., and Cowtan, K. (2004) Coot: model-building tools for molecular graphics. *Acta Crystallogr., Sect. D: Biol. Crystallogr. 60* (12), 2126−2132.
(27) DeLano, W. (2002) *The PyMOL Molecular Graphics System*, DeLano Scientific, San Carlos, CA, USA.
(28) Krissinel, E., and Henrick, K. (2007) Inference of macromolecular assemblies from crystalline state. *J. Mol. Biol. 372* (3), 774−797.
(29) Dundas, J., Ouyang, Z., Tseng, J., Binkowski, A., Turpaz, Y., and Liang, J. (2006) CASTp: computed atlas of surface topography of proteins with structural and topographical mapping of functionally annotated residues. *Nucleic Acids Res. 34* (S2), W116−W118.

DOI: 10.1021/acsinfecdis.7b00068
ACS Infect. Dis. 2017, 3, 653−665